

## Insight into the Selectivity of Isopropanol Conversion at Strontium Titanate (100) Surfaces: A Combination Kinetic and Spectroscopic Study

Shuai Tan, Matthew B. Gray, Michelle K. Kidder, Yongqiang Cheng, Luke L. Daemen, Dongkyu Lee, Ho Nyung Lee, Ying-Zhong Ma, Benjamin Doughty, and Daniel A. Lutterman

*ACS Catal.*, **Just Accepted Manuscript** • DOI: 10.1021/acscatal.7b02417 • Publication Date (Web): 13 Oct 2017

Downloaded from <http://pubs.acs.org> on October 13, 2017

### Just Accepted

“Just Accepted” manuscripts have been peer-reviewed and accepted for publication. They are posted online prior to technical editing, formatting for publication and author proofing. The American Chemical Society provides “Just Accepted” as a free service to the research community to expedite the dissemination of scientific material as soon as possible after acceptance. “Just Accepted” manuscripts appear in full in PDF format accompanied by an HTML abstract. “Just Accepted” manuscripts have been fully peer reviewed, but should not be considered the official version of record. They are accessible to all readers and citable by the Digital Object Identifier (DOI®). “Just Accepted” is an optional service offered to authors. Therefore, the “Just Accepted” Web site may not include all articles that will be published in the journal. After a manuscript is technically edited and formatted, it will be removed from the “Just Accepted” Web site and published as an ASAP article. Note that technical editing may introduce minor changes to the manuscript text and/or graphics which could affect content, and all legal disclaimers and ethical guidelines that apply to the journal pertain. ACS cannot be held responsible for errors or consequences arising from the use of information contained in these “Just Accepted” manuscripts.



1  
2  
3  
4  
5  
6  
7  
8  
9  
10  
11  
12  
13  
14  
15  
16  
17  
18  
19  
20  
21  
22  
23  
24  
25  
26

# Insight into the Selectivity of Isopropanol Conversion at Strontium Titanate (100) Surfaces: A Combination Kinetic and Spectroscopic Study

27  
28  
29  
30  
31  
32  
33  
34  
35  
36  
37  
38  
39  
40  
41  
42  
43  
44  
45  
46  
47  
48  
49  
50  
51  
52  
53  
54  
55  
56  
57  
58  
59  
60

*Shuai Tan<sup>1</sup>, Matthew B. Gray<sup>2</sup>, Michelle K. Kidder<sup>1</sup>, Yongqiang Cheng<sup>3</sup>, Luke L. Daemen<sup>3</sup>,  
Dongkyu Lee<sup>4</sup>, Ho Nyung Lee<sup>4</sup>, Ying-Zhong Ma<sup>1</sup>, Benjamin Doughty<sup>1,\*</sup> and Daniel A.  
Lutterman<sup>1,\*</sup>*

#### AUTHOR ADDRESS:

1. Chemical Sciences Division, Oak Ridge National Laboratory, Oak Ridge, TN, 37831, USA
2. Department of Chemistry and Biochemistry, Ohio State University, Columbus, Ohio 43210, United States
3. Chemical and Engineering Materials Division, Neutron Sciences Directorate, Oak Ridge National Laboratory, Oak Ridge, TN, 37831, USA
4. Materials Science and Technology Division, Oak Ridge National Laboratory, Oak Ridge, TN, 37831, USA

Notice: This manuscript has been authored by UT-Battelle, LLC under Contract No. DE-AC05-00OR22725 with the U.S. Department of Energy. The United States Government retains and the publisher, by accepting the article for publication, acknowledges that the United States Government retains a non-exclusive, paid-up, irrevocable, world-wide license to publish or reproduce the published form of this manuscript, or allow others to do so, for United States Government purposes. The Department of Energy will provide public access to these results of federally sponsored research in accordance with the DOE Public Access Plan (<http://energy.gov/downloads/doe-public-access-plan>).

**Abstract:**

This work aims to better understand the role of interfacial molecular structure that governs selectivity and activity in heterogeneous catalytic reactions. To address this, a comprehensive study of isopropanol conversion over an archetypal perovskite material, strontium titanate ( $\text{SrTiO}_3$  or STO), was performed with an array of techniques sensitive to orthogonal aspects of the ensuing chemistry. Cubic-shape STO nanoparticles with only the (100) facet exposed were synthesized and used to study the ensemble kinetic conversion of isopropanol over the surfaces, which showed selectivity to form acetone, with minor propylene products appearing at elevated temperatures. These results in combination with inelastic neutron scattering measurements provide not only insight into the selectivity and overall activity of the catalysts but also low frequency vibrational signatures of the adsorbed and reacted species. To compliment these measurements, pristine thin films of STO (100) were synthesized and used in combination with vibrational sum frequency generation spectroscopy to extract the absolute molecular orientation of the adsorbed molecules at the interface. It was found that the isopropanol assumes an orientation where the -CH group points towards the STO surface; this pre-reaction geometry offers an obvious pathway to produce acetone by abstracting the alpha-proton and, thus, provides a mechanistic explanation of selectivity at STO (100) surfaces. This insight opens up pathways to explore and modify surfaces to tune the activity/selectivity through a molecular level understanding of the reactions at the surface.

**Keywords:**

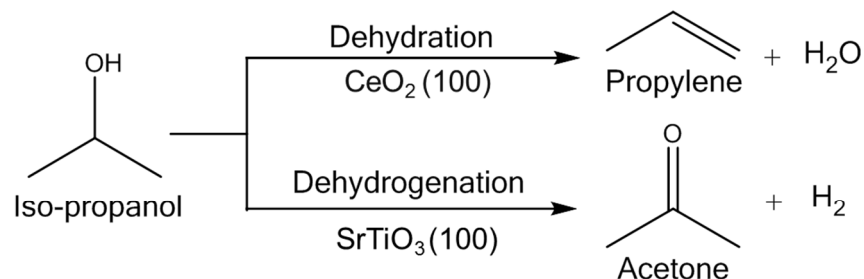
Perovskite, Strontium Titanate, Isopropanol, Neutron Spectroscopy, SFG

**Introduction:**

Understanding how catalyst structure and composition affect product distributions is a long standing goal in the field of heterogeneous catalysis.[1-2] It is thought that with an understanding of how structural organization promotes specific reactivity and selectivity, one could tune the catalytic properties to yield the desired products.[3-4] In a heterogeneous catalytic system, the initial microscopic mechanistic step involves the adsorption of a molecule onto a reactive catalytic surface. A description of the composition, structure, and orientation of the adsorbed molecules on the surface from this initial interfacial interaction can aid in the understanding of how catalysts operate and differentiate selectivity at various surfaces.

In this work, we make use of the reactions of alcohols, which are known to generally proceed via dehydration pathways to produce alkenes and water on acidic oxides or dehydrogenation pathways on basic oxides producing aldehydes and hydrogen (see Scheme 1).[5-7] Recently, we examined isopropanol adsorption on the surface of a model  $\text{CeO}_2$  catalyst that was synthesized with only the (100) facets exposed. We found that isopropanol readily deprotonated at the  $\text{CeO}_2$  (100) surface, and the molecules appears to arrange to a 'pre-reaction' geometry to allow for H-abstraction from a methyl group at elevated temperatures.[8] While  $\text{CeO}_2$  drives isopropanol to produce propylene upon heating through a dehydration mechanism, other metal oxides and bimetallic oxide systems, such as strontium titanate ( $\text{SrTiO}_3$ , referred to here as STO), are known to promote the production of acetone via dehydrogenation.[9] Despite this knowledge, the mechanism underlying the conversion is not well understood, nor is there an obvious reason why

1  
2  
3 the two oxide surfaces would uniquely drive chemistry in the way that they do. The question  
4 is then: How do the structures and orientations of adsorbed molecules differ in these two  
5 systems and what can that tell us about selectivity? To this end, this work aims to elucidate  
6 what governs the specificity of catalysts and what chemistry is uniquely driven using a  
7 combination of neutron scattering, kinetic measurements, and nonlinear optical spectroscopy.  
8  
9  
10  
11  
12  
13  
14



28  
29  
30  
31  
32  
33  
34  
35  
36  
37  
38  
39  
40  
41  
42  
43  
44  
45  
46  
47  
48  
49  
50  
51  
52  
53  
54  
55  
56  
57  
58  
59  
60

Scheme 1. Reaction pathways of iso-propanol over different catalysts.

Neutron spectroscopy is particularly a powerful approach to study heterogeneous catalysis due to the penetrating power of neutrons and their unparalleled sensitivity to light elements and hydrogen,[10] which is important to the reactions studied here. Neutron scattering is an overall underutilized technique in the field of catalysis, due to its infamous reputation for requiring large sample sizes and long collection times for measurements. However, the neutron flux at the Spallation Neutron Source (SNS) at Oak Ridge National Laboratory is 4000 times greater than any of its predecessors, which enables us to attain higher resolution spectra in shorter amounts of time with smaller sample sizes than ever before.[11] As we will show below, applying inelastic neutron scattering spectroscopy to catalytic questions provides a wealth of information regarding the structure and dynamic of adsorbates at the catalyst surface during the reaction. This information together with reaction kinetics provide the macroscopic performance and selectivity of STO nanocube catalysts, which offer new insight into the origin of the activity and selectivity of the surfaces. To

1  
2  
3 evaluate the molecular orientation at the interfaces, we employ vibrational sum-frequency  
4 generation (SFG), a surface specific nonlinear optical probe capable of providing absolute  
5 molecular orientation at surfaces.[12-20] Through this comprehensive approach, we can directly  
6  
7  
8 correlate the pre-reaction orientations of isopropanol extracted via SFG and the  
9  
10 activity/selectivity of these nanoshape surfaces with the same exposed facets using neutron  
11  
12 scattering and kinetic measurements to *understand* the molecular scale events that drive  
13  
14 selectivity at catalytic interfaces.  
15  
16  
17  
18  
19  
20  
21  
22  
23

## 24 **Experimental Details:**

### 25 **Materials Synthesis:**

26  
27 The following chemicals were used as received: Strontium oxalate dihydrate ( $\text{SrC}_2\text{O}_4 \cdot 2\text{H}_2\text{O}$ ,  
28 99%, Alfa Aesar), Titanium Oxide-anatase ( $\text{TiO}_2$ , 99.9%, Aldrich Chemical), Sodium Chloride  
29  
30 (NaCl, 99%, Fisher Chemical)  
31  
32  
33

34  
35  
36  $\text{SrTiO}_3$  cuboidal nanoparticles were synthesized via a modified molten salt process described  
37  
38 in Stair *et al.*[21] Briefly, a mixture of  $\text{SrC}_2\text{O}_4 \cdot 2\text{H}_2\text{O}$ :  $\text{TiO}_2$ : NaCl in a 1:1:20 molar ratio was  
39  
40 rigorously ground in a mortar and a pestle and loaded into a crucible. The sample was heated to  
41  
42 850 °C in air for 4 hours followed by cooling down to room temperature. The resulting powder  
43  
44 was then washed with excess deionized  $\text{H}_2\text{O}$  in order to remove NaCl, and subsequently dried in  
45  
46 an oven at 110 °C overnight. Commercial STO powders (99%, Sigma Aldrich) were purchased  
47  
48 and used after calcination at 550 °C for 4 hours.  
49  
50  
51  
52

53 In order to obtain a well-defined and flat surface for nonlinear optical measurements,  $\text{SrTiO}_3$   
54  
55 (100) single-crystalline substrates were chemically and thermally treated. First the samples were  
56  
57  
58  
59  
60

1  
2  
3 chemically etched in buffered hydrofluoric acid for 30 seconds to obtain a TiO<sub>2</sub>-terminated  
4 surface, followed by thermal annealing at 1000 °C in air for 90 minutes to develop an atomically  
5 smooth surface (see Supporting Information, Figure S1) characterized by atomic force  
6 microscopy (AFM) measurement.[22]  
7  
8  
9  
10  
11  
12  
13  
14

### **Characterization Methods:**

15  
16

17 XRD patterns were measured with an X'pert Pro X-ray diffractometer from PANalytical  
18 with nickel-filtered Cu K $\alpha$  radiation ( $\lambda = 1.5418 \text{ \AA}$ ), with generator setting of 40 mA and 45  
19 kV. The scanning region was set to be 10 - 90° with a step size of 0.025°.  
20  
21  
22  
23

24 Specific surface area was determined by N<sub>2</sub> adsorption-desorption isotherms carried out  
25 with a Quantachrome 1C Autosorb. About 0.1 g of sample was outgassed with helium at  
26 150 °C for 5 h.  
27  
28  
29  
30

31 Scanning electron microscope (SEM) was performed using a Hitachi HD-  
32 2000 equipment operating at 200 kV. Samples were loaded onto a 300 mesh copper grid with  
33 lacey carbon backing.  
34  
35  
36  
37

38 Atomic force microscopy (AFM) was used to examine the surface morphology of (100)  
39 SrTiO<sub>3</sub> single-crystalline substrates. An atomically flat surface was observed with a root-  
40 mean-square (RMS) roughness value below 0.1 nm.  
41  
42  
43  
44

45 Inelastic neutron scattering (INS) measurements were carried out on beamline 16B, the  
46 Vibrational Spectrometer (VISION) at the Spallation Neutron Source, at Oak Ridge National  
47 Laboratory. VISION is a high-flux high-throughput INS instrument covering a broad energy  
48 range from -2 to 1000 meV.[23] In these experiments, about 3 g of sample was loaded into a  
49 home-built cylindrical quartz reactor. The reactor was sealed and heated under vacuum at  
50  
51  
52  
53  
54  
55  
56  
57  
58  
59  
60

1  
2  
3 120 °C overnight until the measured pressure was below  $1 \times 10^{-6}$  mbar to remove air and loosely  
4 bound surface H<sub>2</sub>O prior the measurement. The INS spectra of pure materials, including the  
5 nanocatalyst, bulk phase of Isopropanol (IPA)/acetone/propylene were measured by adding  
6 sample into the empty reactor. Adsorbates were added to the catalysts held at 30 K within a time  
7 span of 5 - 10 min. The adsorbate was dosed via a capillary into the sample can using a home-  
8 built gas-manifold. Our INS measurements were carried out at 5 K and started roughly 20 min  
9 after loading. Additional experimental conditions are provided specifically in the Results section.  
10 To isolate the adsorption and subsequent reactions of molecules at the nanocube surfaces, the  
11 background, which is the signal of the pure materials, were subtracted. INS spectra were  
12 collected with neutron energy loss up to energy transfer values of 1000 meV, corresponding to  
13 about 8000 cm<sup>-1</sup>.  
14  
15  
16  
17  
18  
19  
20  
21  
22  
23  
24  
25  
26  
27  
28

29 Sum-frequency generation (SFG) spectroscopy was performed using a home-built  
30 spectrometer described in detail elsewhere.[8, 24-25] Briefly, isopropanol was drop cast on  
31 pristine STO (100) surface allowed to dry in atmosphere before SFG measurements commenced.  
32 Adsorption of species from the atmosphere was previously found to not impact the spectra or  
33 orientational results in a meaningful way.[8] The SFG spectra were collected in three  
34 polarization combinations denoted as SSP, PPP, and SPS. Following convention, the  
35 polarization combinations describe the radiated SFG (S-), incident near-infrared (S-), and mid-IR  
36 pulses (P-), light fields, respectively. Transition frequencies and amplitudes that characterize the  
37 molecules at the surface are extracted by fitting the data to equation 1:[26]  
38  
39  
40  
41  
42  
43  
44  
45  
46  
47  
48  
49  
50

$$I_{SFG} = \left| A_{NR} + \sum_q^n \frac{A_q}{\omega_{IR} - \omega_q + i\Gamma_q} \right|^2 \quad (\text{eq. 1})$$

51 where  $I_{SFG}$  represents the measured SFG signal,  $A_{NR}$  is a non-resonant contribution to the SFG  
52 signal,  $A_q$  is the amplitude of the  $q^{\text{th}}$ -resonance,  $\omega_{IR}$  and  $\omega_q$  are the frequencies of the incident  
53  
54  
55  
56  
57  
58  
59  
60

1  
2  
3 light and the vibrational resonance, respectively, and  $\Gamma_q$  is the linewidth. Fitting to more  
4  
5 complex functions, such as a Voigt profile, was not attempted due to the increased number of  
6  
7 freely adjustable parameters which would result in over fitting the data. [27]  
8  
9

### 10 11 12 **Activity Tests:**

13  
14  
15 Isopropanol (IPA) conversion reactions were carried out in a 1/4-inch diameter tubular  
16  
17 quartz reactor. In a typical run, ca. 30 mg catalysts was mixed with 370 mg 60-80 mesh  
18  
19 quartz sand and loaded in the reactor. The catalyst bed was held by quartz wool at both ends.  
20  
21 The reactor was inserted to Carbolite-Gero furnace (MTF10-15-130), and purged with 50  
22  
23 sccm Ar flow for 0.5 h, followed by heating to desired temperature (i.e., 300 °C). For the  
24  
25 activation treatment procedure, a 50 sccm, 10 % O<sub>2</sub>/Ar flow was applied for 1 h at 550 °C,  
26  
27 followed by 50 sccm Ar flow purge for 5 min. The IPA was injected to the heated gas line  
28  
29 with syringe pump (The New Era Pump Systems Inc.) at various rates. The gas line was  
30  
31 wrapped with heating cord, which is set to 95 °C in order to ensure the IPA stays fully  
32  
33 vaporized throughout the path to the reactor.  
34  
35  
36  
37

38  
39 The samples were analyzed on line by a Buck Scientific 910 gas chromatograph equipped  
40  
41 with a Restek Packed Column (15% CW-20M, 6 ft, 2 mm I.D., 1/8 in O.D.) and a flame  
42  
43 ionization detector (FID), respectively. After the reaction, the catalyst was purged with Ar,  
44  
45 cooled to room temperature, removed from the reactor and saved in a glass vial for additional  
46  
47 characterization.  
48  
49

50  
51 The conversion and selectivity were calculated by using the following equations:

52  
53  
54 
$$IPA\ Conversion\ (\%) = \frac{\sum X_{i,out}}{\sum X_{i,out} + IPA_{out}} \times 100\% \quad (eq.2)$$

55  
56  
57 
$$Selectivity\ (\%) = \frac{X_{i,out}}{\sum X_{i,out}} \times 100\% \quad (eq. 3)$$

whereas  $X_{i,\text{out}}$  refers to concentration of the  $i^{\text{th}}$  product (i.e.,  $\text{CO}_2$ , propylene, acetone), and  $\text{IPA}_{\text{out}}$  is the concentration of IPA measured in the exit port.

## Results and Discussion

Figure 1 shows the XRD patterns of the synthesized and commercial STO catalysts. It can be seen that for the cubic STO sample, peaks were apparent at  $32.6^\circ$ ,  $39.9^\circ$ ,  $46.5^\circ$ ,  $57.9^\circ$ ,  $67.9^\circ$ , and  $77.2^\circ$ , which are assigned to  $\text{SrTiO}_3$  (JCPDS: 35-0734). It should be mentioned that a commercial STO sample shows almost identical XRD peaks, except one shoulder peak at ca.  $31.6^\circ$ . This is possibly due to presence of other phase, such as  $\text{Sr}_2\text{TiO}_4$  (JCPDS: 39-1471) and  $\text{Sr}_3\text{Ti}_2\text{O}_7$  (JSCPD: 11-0663).

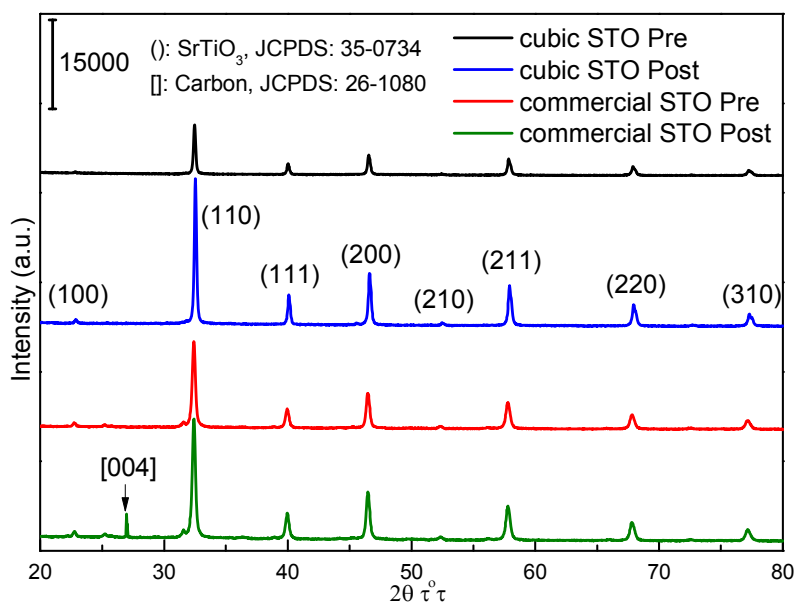


Figure 1. XRD patterns of synthesized cubic STO and commercial STO, before and after reactions.

1  
2  
3 The morphology of STO samples was determined by SEM. As can be seen in Figure 2,  
4 the as synthesized STO sample has a roughly cubic shape, with ca. 100 - 200 nm diameter  
5 (Figure 2a). It should be mentioned that cubic STO samples have primarily (100) face  
6 exposed due to the low surface energy with only a small fraction of (110) sites at the  
7 corner.[21, 28] In contrast, the commercial STO powder has inhomogeneity particle sizes  
8 with irregular shapes. These particles are without well-defined surface facets exposed (Figure  
9 2c).  
10  
11  
12  
13  
14  
15  
16  
17  
18  
19  
20  
21  
22  
23  
24  
25  
26  
27  
28  
29  
30  
31  
32  
33  
34  
35  
36  
37  
38  
39  
40  
41  
42  
43  
44  
45  
46  
47  
48  
49  
50  
51  
52  
53  
54  
55  
56  
57  
58  
59  
60

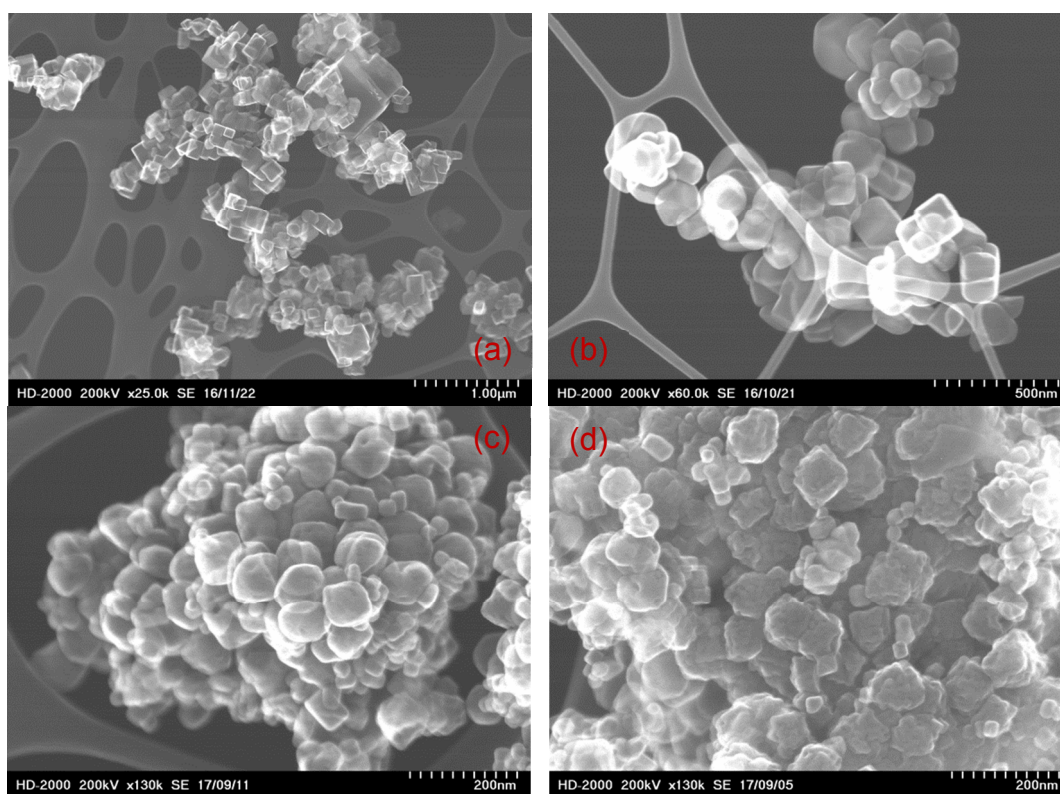


Figure 2. SEM images of synthesized cubic STO sample (a) before and (b) after 6 h reaction, and commercial STO sample (c) before and (d) after 6 h reaction.

The textural properties (i.e., surface area etc.) of the commercial and synthesized cubic STO, are determined from  $N_2$ -physisorption isotherms (Figure 3). In short, both the

commercial and synthesized STO are nonporous material. However, the surface area of the commercial sample is over 3-fold larger than the cubic STO (24 vs. 7 m<sup>2</sup>/g). As the surface area of STO is strongly structure-dependent, the low value for cubic STO is likely due to the flat exposed facets, whereas the irregular and rough surfaces of commercial STO lead to a high value.

As depicted in Figure 3, both these materials show very low adsorption over a wide relative pressure regime. Such phenomenon indicates that there is no identifiable monolayer formation and show stronger adsorbate-adsorbate interaction rather than adsorbate-adsorbent interaction. Hence, the isotherms of the STO samples can be identified as type III, which is characteristic of nonporous materials.[29] In addition, type H3 hysteresis loops, according to IUPAC, were detected in all catalysts. This type of loop is characteristic of metastability of the adsorbed multilayer and delayed capillary condensation.[30]

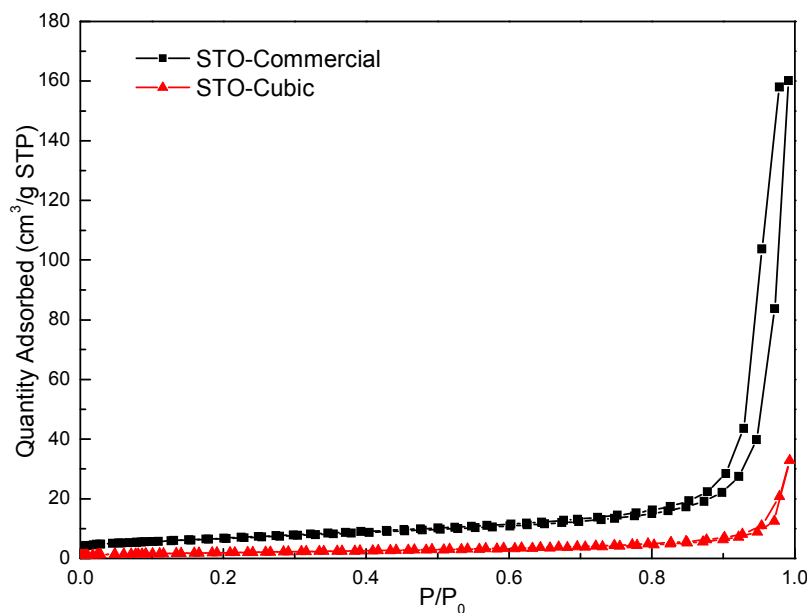


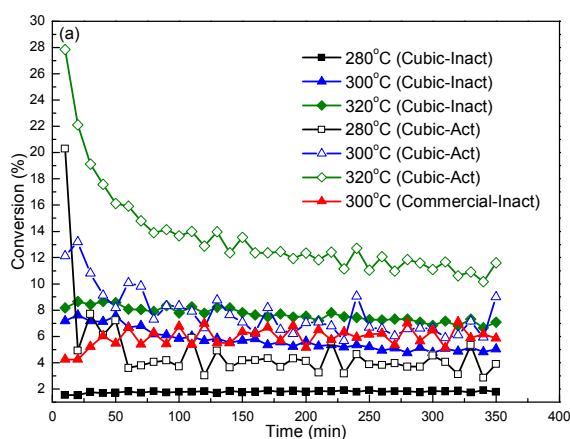
Figure 3. N<sub>2</sub>-physorption isotherms of the commercial and cubic SrTiO<sub>3</sub> samples.

1  
2  
3  
4 Prior to the catalytic tests, control experiments were performed in an empty tube, and  
5  
6 over quartz sand under the same reaction conditions. All experiments had ca. 1.2 s residence  
7  
8 times. The background IPA conversion was negligible.  
9

10  
11  
12 The catalytic performance of cubic and commercial STO samples with/without activation  
13  
14 of catalyst is shown in Figure 4. To start, we consider the conversion of IPA over the  
15  
16 synthesized cubic nanocatalysts at 280 °C without activation, as shown in Figure 4a (black  
17  
18 solid symbol). Here, we find that the conversion is ca. 2 %, with the acetone being the only  
19  
20 product (Figure 4b, black solid symbol being overlapped by black open symbol). As the  
21  
22 temperature increased to 300 °C and 320 °C, the conversion rises to 6 % and 8 %,  
23  
24 respectively (solid blue and green symbols in Figure 4a), for the cubic nanocatalysts. In all  
25  
26 cases, acetone was observed as the major product (Figure 4b) with up to 10 % propylene  
27  
28 selectivity (Figure 4c) at the highest temperatures (320 °C). The change in catalytic  
29  
30 selectivity at elevated temperatures indicates an increase of the dehydration pathway at  
31  
32 elevated temperatures, where the intermediate formed at the STO surface can be transformed  
33  
34 to propylene. In contrast, the catalytic performance of commercial STO was found to yield  
35  
36 roughly the same conversion level as compared to the inactivated cubic STO, but remarkably  
37  
38 different selectivities at 300 °C. To be specific, the commercial STO sample shows ca. 63 %  
39  
40 acetone and 37 % propylene, while cubic STO shows 94 % acetone, and 6 % propylene.  
41  
42 Taking into the account that the surface area of commercial STO is ca. 3 times larger than  
43  
44 that of cubic STO, it indicates that the cubic sample exhibits superior activity in at least 3-  
45  
46 fold and is highly acetone-selective. Taking the morphology into account, the differences in  
47  
48 selectivity also point to the role of different facets in driving the chemistry to form acetone at  
49  
50  
51  
52  
53  
54  
55  
56  
57  
58  
59  
60

the (100) facets in the nanocube samples, whereas the presence of different facets on the more rounded edges of the commercial sample likely results in different chemical environments that uniquely drive the chemistry and thus explains the breadth of the product distribution observed.

As a comparison, in a separate experiment, an O<sub>2</sub>-activation step (50 sccm 10% O<sub>2</sub>/Ar flow for 1 h at 550 °C, followed by purged with 50 sccm Ar flow for 10 min) was applied to the catalysts prior the reaction, and the data was also shown in Figure 4 (legends with “-Act”). It should be also mentioned that, for cubic STO samples, such activation could enhance the conversion and acetone selectivity. However, the IPA conversion rapidly dropped to steady level within the first 60 - 120 min. This could be explained by the quick consumption of surface oxygen species as well as residual O<sub>2</sub> in system. The higher level of acetone selectivity is possibly due to the enhancement of dehydrogenation pathway in the “oxidative environment” as proposed in Vedrine’s work.[31] However, a detail study on the effect of such an “activation step” is still needed.



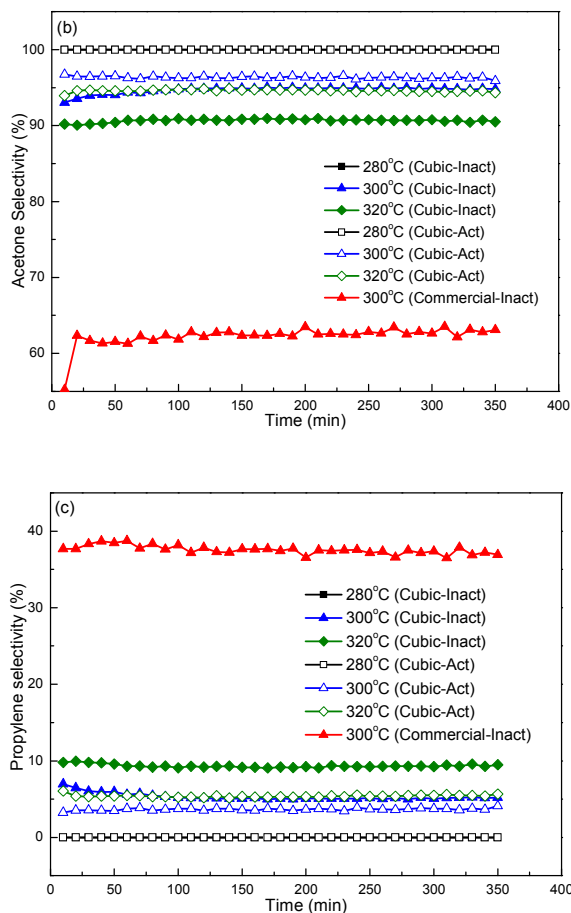
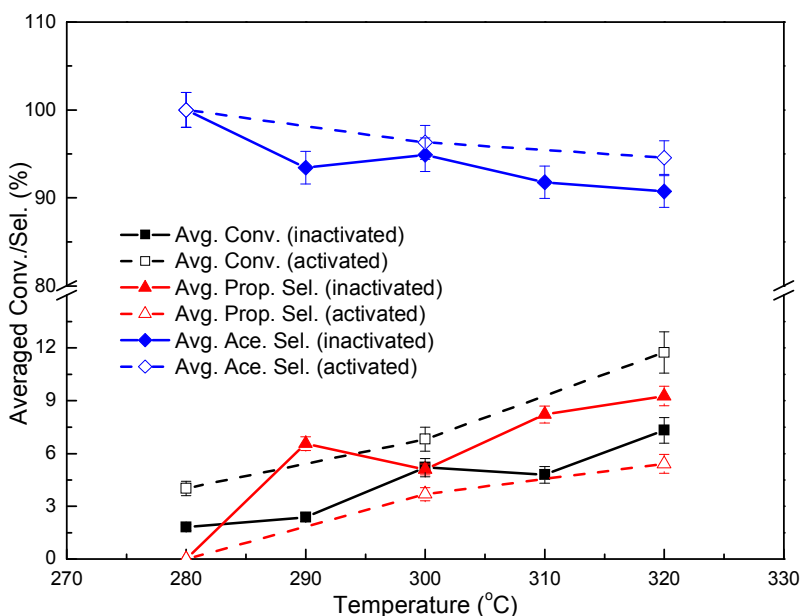


Figure 4. (a) IPA conversion, (b) Acetone selectivity and (c) Propylene selectivity over the synthesized cubic and commercial STO catalysts. Reaction conditions: 30 mg catalysts mixed with 370 mg quartz sand, 1  $\mu$ L/min IPA injection rate, 50 sccm Ar flow, and 1 atm total pressure.

The reacted samples were examined after experiments to see how the chemistry impacted the structure and composition of the materials. Accordingly, both cubic and commercial STO sample were re-characterized (data given in Figure 1). The results indicate that the synthesized nanocube STO samples remain unchanged based on observation of the peaks at the same positions, whereas the commercial samples show new XRD peaks, indicative of the

possible deposition of carbon (JCPDS: 26-1080) on the surface (see arrow in Figure 1), which is likely formed during the reaction. The samples were also re-examined by SEM for structural comparison. As shown in Figure 2b and 2d, these results reveal that the synthesized STO remained nearly ideally cubic with slightly truncated corners, whereas the commercial STO powder shows inhomogeneous particle sizes and shapes.

The temperature effect on the catalytic performance was also studied and the results were shown in Figure 5. As can be seen, regardless of pretreatment, increasing temperature from 280 °C to 320 °C, leads to an increase of both conversion and propylene selectivity, while acetone selectivity suffers a slight drop for the same temperature change. It should be mentioned that, each point is the average of nine measurements. There is generally less than 5% difference of the original value due to systematic error. Again, the activated samples exhibit a higher conversion and acetone selectivity but a lower propylene selectivity than that of inactivated sample, which is consistent with the observation depicted in Figure 4.

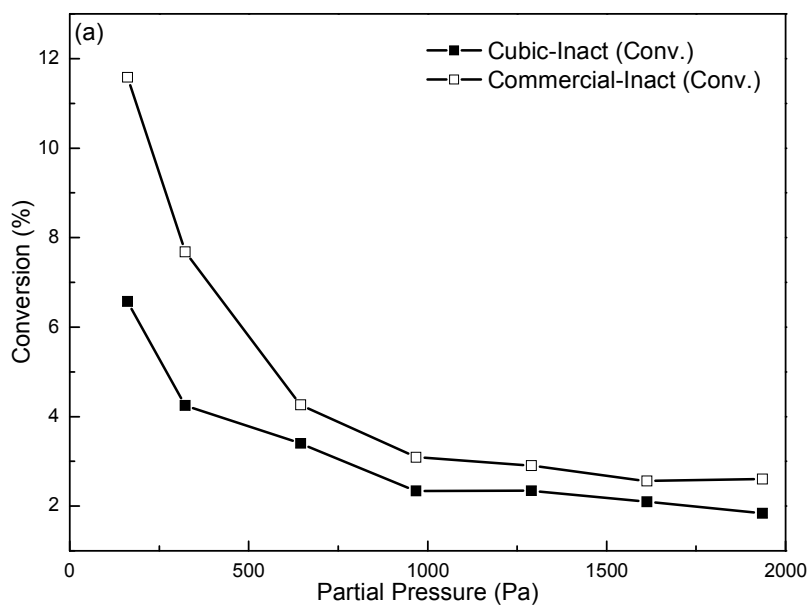


1  
2  
3 Figure 5. Temperature effect on IPA (squares) conversion, Propylene (triangles) and Acetone  
4 (diamonds) selectivity over inactivated (solid symbols) and activated (open symbols) cubic STO  
5 catalyst. Reaction conditions: 30 mg catalysts mixed with 370 mg quartz sand, 1  $\mu\text{L}/\text{min}$  IPA  
6 injection rate, 50 sccm Ar flow, and 1 atm total pressure.  
7  
8  
9  
10  
11  
12  
13  
14

15 In the kinetic analysis of a gas phase-involved reaction, partial pressure could  
16 conveniently substitute for concentration at constant temperature. Accordingly, the effect of  
17 IPA partial pressure (due to different IPA injection rate) over commercial/synthesized STO  
18 was also investigated and the results are summarized in Figure 6. It can be seen that an  
19 increase of partial pressure leads to a drop in conversion in both cases. This might be due to  
20 the increase of WHSV (weight hour space velocity). Once the partial pressure is above 1000  
21 Pa, the conversion reaches a steady level. Meanwhile, the acetone selectivity significantly  
22 increases from 48 % to 68 % within the partial pressure range for the commercial STO  
23 sample, while propylene selectivity decreases. The observed effect is not so obvious with  
24 respect to selectivity over cubic STO, although a slight change is seen. Such a phenomenon  
25 suggests that high population of IPA at the catalyst surface (high partial pressure) leads to an  
26 increase of dehydrogenation pathway (to produce acetone). With the current data alone, one  
27 cannot conclude a simple reason that causes such behavior. For one reason, it is difficult to  
28 quantitatively measure the coverage of IPA over STO surface. In addition, the generated  
29 inter-molecular interaction (e.g., H-bonding) may also change the surface orientation.  
30 However, it is commonly accepted that the selectivity is somehow coverage dependent.[32-  
31 34] In this case, an increasing of injection rate leads to IPA to be more packing at the surface  
32 and overall different possible orientations that the functional groups can take at the surface.  
33  
34  
35  
36  
37  
38  
39  
40  
41  
42  
43  
44  
45  
46  
47  
48  
49  
50  
51  
52  
53  
54  
55  
56  
57  
58  
59  
60

Consequently, as such, the branching between dehydration and dehydrogenation pathways could potentially change as a function of IPA coverage. This remains an open topic for continued investigation at controlled pressures.

Wachs and co-workers have investigated methanol and isopropanol conversion over a variety of metal oxides, and found that the average active site density of SrO and TiO<sub>2</sub> (the two possible termination surfaces of STO) to be 4.3 and 3.7  $\mu\text{mol}/\text{m}^2$ , respectively.[35-36] Taking the surface area into account, the turnover frequency (TOF) can be determined by normalizing the activity under differential conversion regime ( $< 15\%$ ). Hence, the TOF at each IPA partial pressure under 300 °C was calculated from Figure 6. The best TOFs for IPA conversion for cubic and commercial STO are 0.0143 and 0.0059  $\text{s}^{-1}$ , respectively (IPA partial pressure is 1934 Pa).



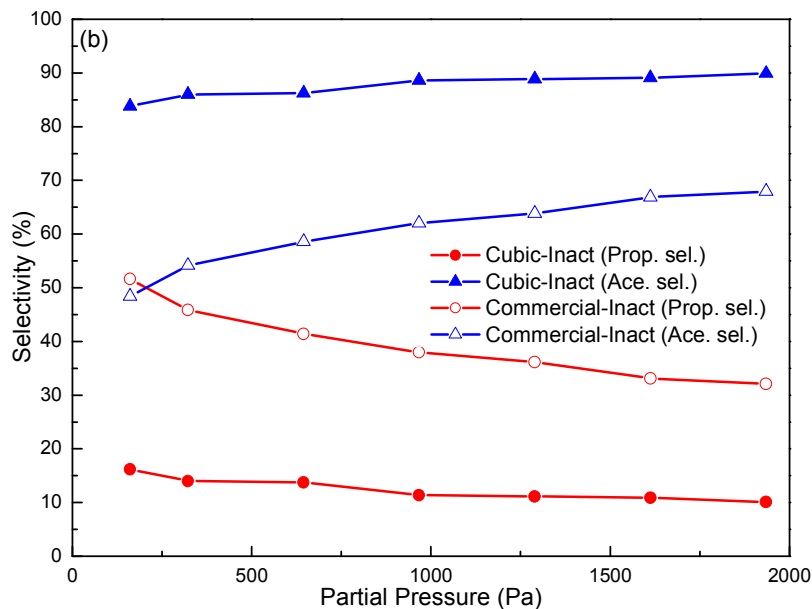
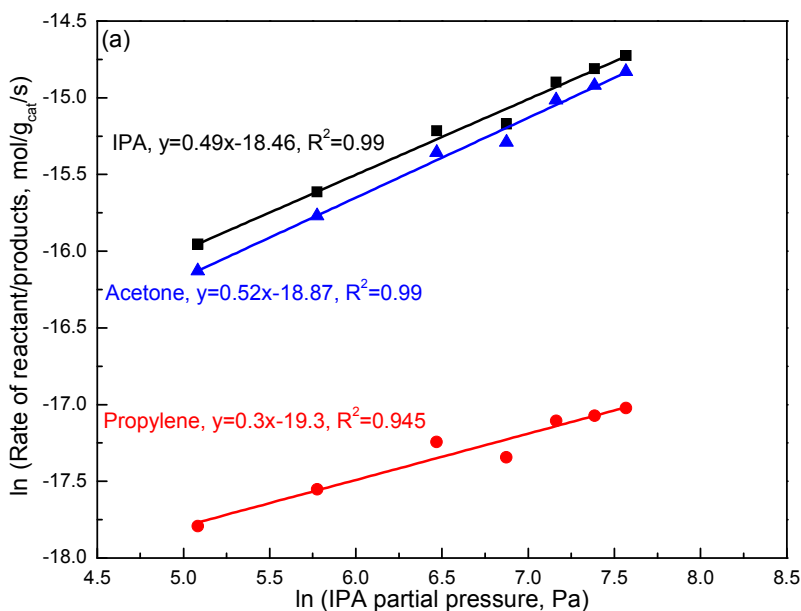


Figure 6. Partial pressure effect on (a) IPA conversion, and (b) Propylene (circles) and Acetone (triangles) selectivity over inactivated cubic STO (solid symbols) and commercial STO (open symbols). Reaction conditions: 30 mg catalyst mixed with 370 mg quartz sand, 0.25 ~ 3  $\mu\text{L}/\text{min}$  IPA injection rate, 50 sccm Ar flow, 300  $^{\circ}\text{C}$ , and 1 atm total pressure.

A plot of logarithm pressure versus logarithm rate allows us to determine the overall order of the reaction (the slope of linear fitting equation), as well as to identify individual production formation channel. As can be seen from Figure 7, the apparent reaction order of IPA, acetone, and propylene over the cubic STO at 300  $^{\circ}\text{C}$  is 0.49, 0.52, and 0.3, respectively. While the corresponding values for the commercial STO case are 0.36, 0.49, and 0.17, respectively. Although the observed reaction orders are slightly different for both type of catalysts, the reaction orders for IPA consumption, as well as acetone formation order appears to be approximately 0.5. There is certain debate regarding the reaction mechanism (derived from the reaction order) of isopropanol decomposition. For example, Vedrine

1  
2  
3 proposed a Langmuir-Hinshelwood kinetics for dehydration of IPA over  $\text{Nb}_2\text{O}_5$ , based on the  
4 observation of propylene reaction order being 1 at low partial pressure, and 0 at high partial  
5 pressures ( $> 2$  kPa).[31] In contrast, Lorenzelli *et al.* proposed a Mars-van Krevelen mechanism  
6 of IPA oxidation over  $\text{Co}_3\text{O}_4$  and  $\text{MgCr}_2\text{O}_4$ , with evidence of nucleophilic lattice oxygen being  
7 involved in the reaction.[37] Moreover, Barteau and co-workers found a 0.5 order with respect to  
8 IPA up to 16 kPa partial pressure over anatase  $\text{TiO}_2$ . [38] Notice that most studies are over single  
9 metal oxides, and only few reports have been focused on decomposition of vapor phase IPA over  
10 perovskite materials.[39]



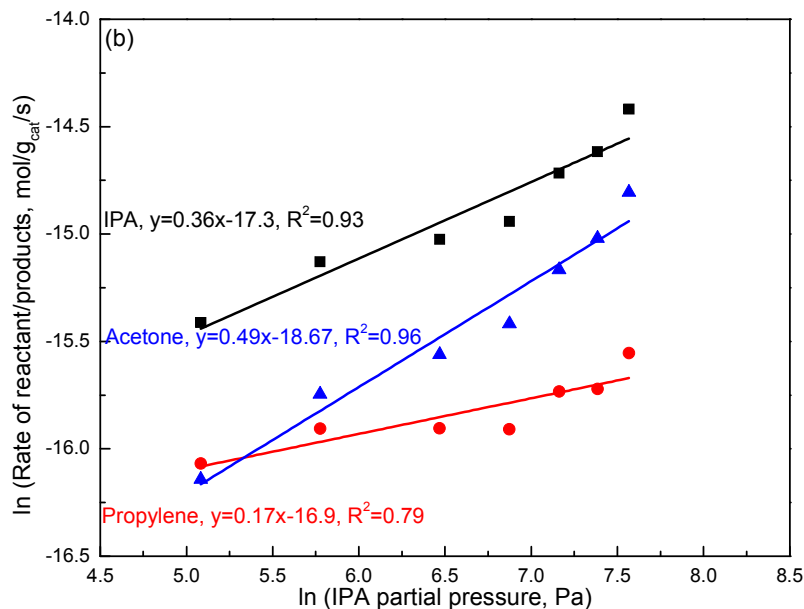


Figure 7. Reaction order of IPA (squares), Propylene (circles) and Acetone (triangles) over (a) cubic STO and (b) commercial STO. Reaction conditions: 30 mg catalyst mixed with 370 mg quartz sand, 0.25 ~ 3  $\mu\text{L}/\text{min}$  IPA injection rate, 50 sccm Ar flow, 300  $^{\circ}\text{C}$ , and 1 atm total pressure.

Since neutron scattering methods are exquisitely sensitive to hydrogen containing molecules and vibrations, INS serves as an ideal platform for the chemistry study of hydrocarbons over a reactive nanocatalysts. Here, we employ INS to measure the surface chemistry during IPA conversion at cubic STO surfaces. Figure 8 shows the spectrum of IPA adsorbed on cubic STO surface. Before the adsorption experiment, the overall signals from bulk phase of STO and IPA, including the sample container and equipment (Aluminum) background were measured separately as references and were subtracted from the IPA adsorption spectra. It can be seen that the bulk IPA gives rise to several characteristic peaks at positions of ca. 239, 280, 373, 492, and 934  $\text{cm}^{-1}$ . The detail vibrational modes are

described in Supporting Information (Figure S2). In contrast pure cubic STO does not show peaks at these positions. For the spectrum acquired with 10  $\mu\text{L}$  IPA adsorbed on STO at 120  $^{\circ}\text{C}$  (already subtracted the bulk STO signal), these characteristic bands due to IPA were observed, indicating surface adsorption of isopropanol.

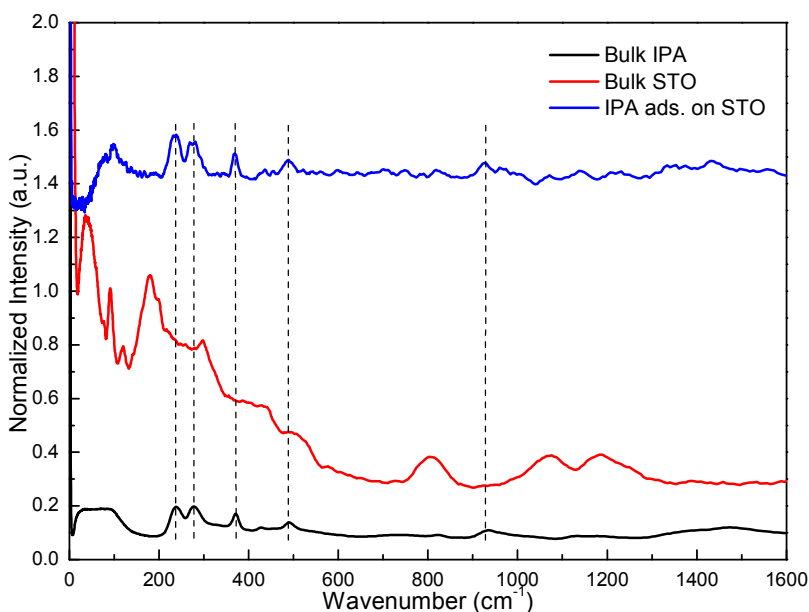
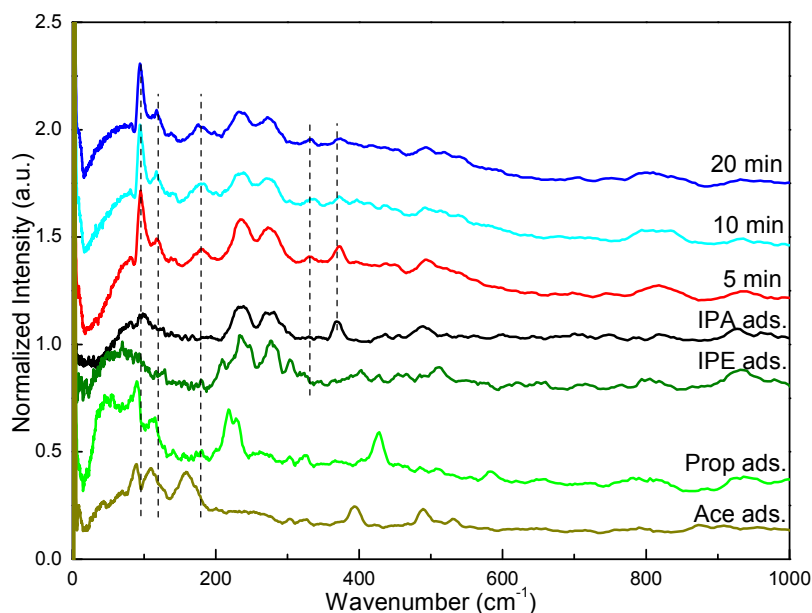


Figure 8. Neutron Vibrational Spectroscopy (NVS) of IPA adsorption on cubic STO.

Next, to study the conversion of IPA over STO nanocatalysts with INS (see Figure 9) we first recorded the INS spectrum from adsorption of possible products (i.e., Propylene (Prop), Acetone (Ace), and Isopropyl Ether (IPE)) to the STO nanocatalysts. Notably, the peak observed at 373  $\text{cm}^{-1}$  is quite unique for IPA, which is absent in product spectra. As such, this band can be used to verify reaction occurrence and IPA consumption. For a reaction taking place at 200  $^{\circ}\text{C}$  for 5 min, the featured bands of IPA remain at a comparable level with respect to the standard spectrum. However, more notably, 3 new bands appear at ca. 116, 180, and 330  $\text{cm}^{-1}$ . They are attributed to propylene/acetone, acetone, and propylene/acetone, respectively. Such observation

1  
2  
3 indicates the occurrence of a reaction. Further heating the sample to 300 °C for an additional  
4  
5 5 min leads to a notable intensity decrease for the peak at 373 cm<sup>-1</sup>, suggesting a further  
6  
7 conversion of IPA. This peak continues to decrease as the reaction proceeds (see spectrum  
8  
9 with another 10 min treatment at 300 °C). Meanwhile, the intensity of the bands at 116, 180,  
10  
11 and 330 cm<sup>-1</sup> increase. Taking into the account the activity results shown above, which  
12  
13 suggests occurrence of certain conversion between 280-320 °C, the new bands measured in  
14  
15 the INS spectra are likely due to the formation of acetone that is adsorbed to the surfaces of  
16  
17 the nanocatalysts. While INS is able to probe the chemical species at the catalyst interface,  
18  
19 molecular level information as to the structure and orientation of the adsorbed molecules at  
20  
21 ambient conditions is difficult to extract from these measurements alone.  
22  
23  
24  
25  
26



48  
49  
50  
51  
52  
53  
54  
55  
56  
57  
58  
59  
60

Figure 9. Neutron Vibrational Spectroscopy (NVS) of IPA reaction over STO. The bulk STO background has been subtracted from all spectra. Reaction temperature: 200 - 300 °C, Spectroscopic measurement temperature: -268 °C.

1  
2  
3 In order to gain insights into catalytic activity/selectivity over cubic STO surface, the  
4 adsorption behavior was investigated by means of SFG in Figure 10. Flat interfaces were used in  
5  
6 SFG measurements to allow for conventional orientational analyses to be applied to the  
7  
8 measured data to extract the absolute molecular orientation of IPA at STO (100) surfaces.  
9  
10 Studies of powdered materials would not allow such a direct analysis due to the symmetry of the  
11  
12 particles and associated complex nonlinear scattering phenomena.[40] However, since the  
13  
14 nanoshapes are predominantly (100) faceted, and the flat STO surface is also (100), the  
15  
16 conclusions and orientational information drawn from the pristine flat interface can be directly  
17  
18 applied to the nanoparticles. Building on recent Raman measurements, SFG experiments with  
19  
20 theoretical support and polarization selection rules, the resolved bands for isopropanol adsorbed  
21  
22 to STO (100) surfaces are assigned. Notably, the spectra observed on STO (100) surfaces are  
23  
24 substantially different from isopropanol on CeO<sub>2</sub> (100) interfaces in both the number of observed  
25  
26 bands as well as the appearance of the spectra. More specifically, in the SSP spectrum many of  
27  
28 the features appear as dips, which are common in SFG measurements of molecules adsorbed  
29  
30 onto the metallic interfaces and are indicative of a different orientation of isopropanol at the  
31  
32 surface of STO vs. CeO<sub>2</sub>. With respect to the SFG spectrum of bare STO, it is well known that in  
33  
34 broadband SFG measurements the response of *any* non-resonant interface matches that of the  
35  
36 driving IR spectrum. As such, the response of the bare STO surface is simply a Gaussian like  
37  
38 spectrum that is scaled out during analysis. Hence, we use a gold film as a reference (see  
39  
40 Supporting Information, Figure S3) simply because it gives a larger signal with better signal-to-  
41  
42 noise than the bare STO itself. By scaling the spectrum by a reference, the wavelength  
43  
44 dependent intensity is intrinsically removed.  
45  
46  
47  
48  
49  
50  
51  
52  
53  
54  
55  
56  
57  
58  
59  
60

1  
2  
3  
4  
5  
6  
7  
8  
9  
10  
11  
12  
13  
14  
15  
16  
17  
18  
19  
20  
21  
22  
23  
24  
25  
26  
27  
28  
29  
30  
31  
32  
33  
34  
35  
36  
37  
38  
39  
40  
41  
42  
43  
44  
45  
46  
47  
48  
49  
50  
51  
52  
53  
54  
55  
56  
57  
58  
59  
60

Similar to our previous work, bands *a* and *f* are assigned to the –CH stretch of isopropanol in agreement with previous DFT calculations[8] and high resolution Raman measurements.[41] We note that the prominent bands at 2943 cm<sup>-1</sup> observed in all three polarization combinations (bands *d*, *j*, and *k*) are readily attributed to the CH<sub>3</sub>-asymmetric stretching (CH<sub>3</sub>-*as*, *r*<sup>-</sup>) modes of deprotonated isopropanol, in agreement with work on CeO<sub>2</sub> (100) surfaces.[8] However, a small feature at ~2960 cm<sup>-1</sup> (bands *e* and *l*) is also observed and is in good agreement with the location of the CH<sub>3</sub>-*as* stretch of protonated isopropanol.[13, 42-43] This observation points towards the coexistence of both protonated and deprotonated isopropanol species at STO (100) surfaces at room temperature. This also means that the STO (100) surface is less basic than the CeO<sub>2</sub> (100) surface, where isopropanol was completely deprotonated. These assignments follow selection rules[12, 42] for asymmetric stretching modes and are in excellent agreement with our previous experiments, analysis, and DFT calculations[8] as well as other literature probing neat isopropanol interfaces.[13, 42-43] Noting that two species are in coexistence at the surface greatly complicates the assignment of bands in the middle of the spectra since features corresponding to the protonated and deprotonated species will overlap. As such, we can only attribute bands *b*, *c*, *g*, *h*, and *i* to some combination of Fermi resonances, CH<sub>3</sub>-symmetric stretching, and –OH stretches in a shared H-bond geometry.[8] It is important to note that in comparing these results to CeO<sub>2</sub>, we achieve two important goals: 1) we show agreement with previous result in terms of band positions for the deprotonated species, while showing the existence of a protonated species, and 2) we show how the two catalysts display different selectivity and how this difference corresponds with the absolute molecular orientation.

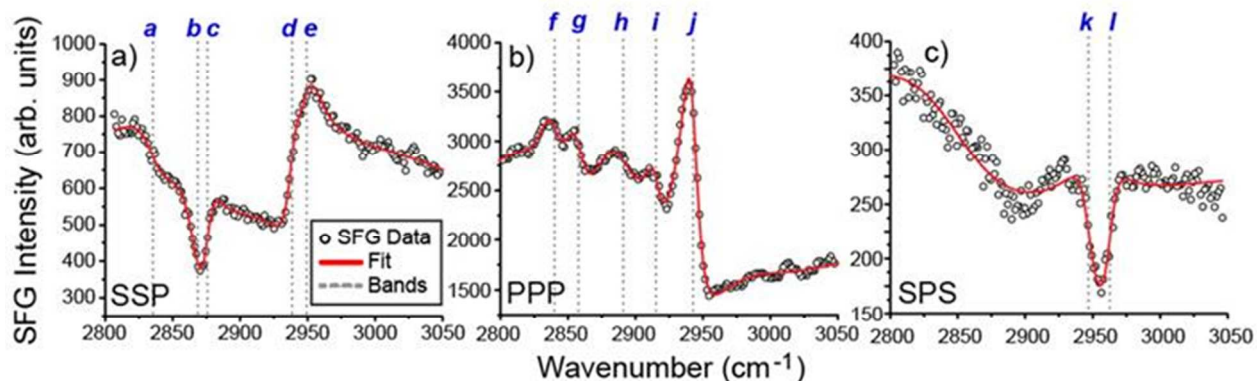


Figure 10. SFG spectra of isopropanol at STO (100) interfaces collected in the SSP (a), PPP (b), and SPS (c) polarization combinations. Bands are labeled as letters from *a-l*.

Having assigned and resolved vibrations from two well defined functional groups on the deprotonated isopropanol structure, we can use the extracted amplitudes to determine the orientations of  $-\text{CH}$  and  $-\text{C}(\text{CH}_3)_2$  functional groups can be determined using the frame work described in our previous work. Briefly, Fresnel factors for the incoming and outgoing light fields were calculated[12, 14, 44] assuming an interfacial index of refraction of 1.18. The choice of the interfacial index to be 1.18 is supported by excellent agreement our previous results on  $\text{CeO}_2$  with theory, along with other reports where 1.18 is a commonly used interfacial index of refraction value for organic species far from electronic resonance.[12, 45-46] The indices of refraction for STO were taken to be 2.38, 2.34, and 2.21 for the SFG, NIR and IR light, respectively.[47] Using the intensity ratio of  $-\text{CH}$  amplitudes obtained in the SSP and PPP spectra the  $-\text{CH}$  bond angle with respect to the surface normal was determined to be  $\theta_{\text{CH}} = 51 \pm 8^\circ$  angle with respect to the surface normal. The methyl groups are treated in by the unified atom model[8, 13] effectively reducing the tetrahedral geometry surrounding the central carbon of isopropanol to trigonal planer structure having  $-\text{CH}$ ,  $-\text{CO}$ , and  $-\text{C}(\text{CH}_3)_2$  groups. Inserting measured intensity ratios for the SSP, PPP, and SPS polarization combinations as extracted for

1  
2  
3 the methyl asymmetric stretch, we can obtain a family of solutions describing possible twist-tilt  
4 angle combinations that the methyl groups could possibly take given the measured data. The  
5  
6 correct twist/tilt angle pair is determined using the constraint that the angle between the  $-CH$  and  
7  
8  $-C(CH_3)_2$  groups is  $120^\circ$  and that the measured orientational angle of the  $-CH$  group be satisfied.  
9  
10 Here we assume the  $-CH$  group is pointed downwards towards the surface such that the angle the  
11  
12  $-CH$  takes is  $90^\circ + 51^\circ = 141^\circ$  and is supported by the dramatically different SFG signals,  
13  
14 particularly in the SSP spectrum, observed here vs. at  $CeO_2(100)$  surfaces, which is indicative of  
15  
16 differing up-down orientations of the functional groups in isopropanol.[46] Applying these  
17  
18 constraints, we arrive at the dashed red lines in Figure 11. The intersection area of the dashed  
19  
20 red lines and solid blue lines represent the allowed angles the methyl groups can take that  
21  
22 simultaneously satisfy the measured  $-CH$  bond angle with respect to the surface normal. From  
23  
24 this analysis, the average orientational twist and tilt angles for the  $-C(CH_3)_2$  group are found to  
25  
26 be  $\psi = 35 \pm 15^\circ$  and  $\theta = 29 \pm 7^\circ$ , respectively. The somewhat large uncertainties in these angles  
27  
28 are a result of challenges in fitting the SFG spectra in the presence of strong non-resonant  
29  
30 contributions with multiple overlapping bands from different chemical species.  
31  
32  
33  
34  
35  
36  
37  
38  
39  
40  
41  
42  
43  
44  
45  
46  
47  
48  
49  
50  
51  
52  
53  
54  
55  
56  
57  
58  
59  
60

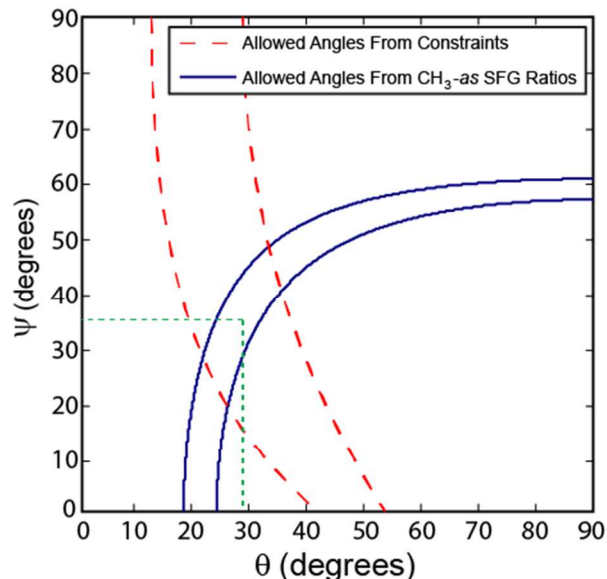
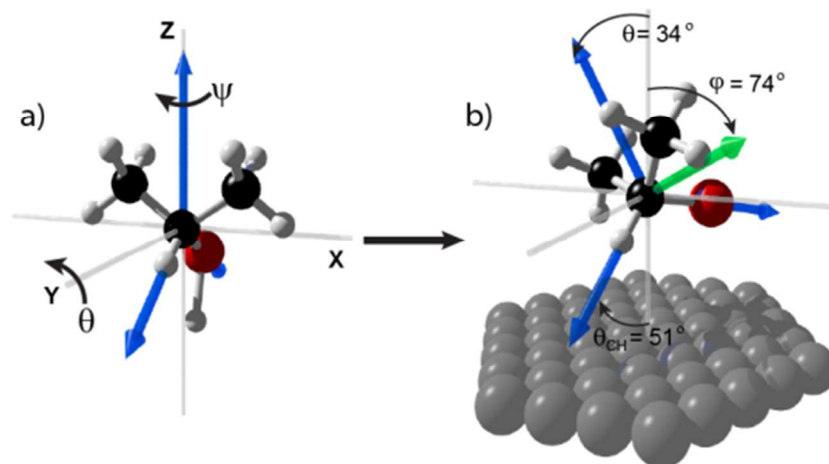


Figure 11. Intersection of possible methyl twist/tilt angles and constraints as defined in the text is used to uniquely determine the orientation of methyl groups. The intersection of these two regions represents the unique simultaneous solution for the measured intensities in SFG experiments.

The absolute molecular orientation is obtained by first defining the molecular orientation such that the  $-\text{C}(\text{CH}_3)_2$  group is pointed in the  $+Z$  direction as shown in Figure. 12a.[8, 48] Blue arrows are unit vectors pointing along the various bond axes/bisector that in turn define the molecular plane. The coordinates of the  $-\text{C}(\text{CH}_3)_2$  group are represented by the direction cosine  $(l_{\text{CH}_3,x}^0, l_{\text{CH}_3,y}^0, l_{\text{CH}_3,z}^0) = (0, 0, 1)$  whereas the  $-\text{CH}$  group is given as  $(l_{\text{CH},x}^0, l_{\text{CH},y}^0, l_{\text{CH},z}^0) = (\cos(-30^\circ), 0, \cos(120^\circ))$ . Next, two consecutive rotations are applied, the first being  $\psi = 35^\circ$  twist about the  $Z$ -axis followed by tilting by  $\theta = 29^\circ$ , about the  $Y$ -axis (sketched in Figure 12a). The laboratory frame direction cosines for the  $-\text{C}(\text{CH}_3)_2$  and  $-\text{CH}$  group are  $(\cos(61^\circ), \cos(90^\circ), \cos(29^\circ))$  and  $(\cos(68^\circ), \cos(60^\circ), \cos(141^\circ))$ , respectively. As necessary, the projection of the  $-\text{CH}$  bond angle with respect to the normal is in agreement with independent orientational

1  
2  
3  
4 analysis. The *absolute* molecular orientation is defined as the angle of the molecular normal  
5  
6 (green arrow in Figure 12b) with respect to the surface normal, which is the cross product of  
7  
8 the rotated  $-C(CH_3)_2$  and  $-CH$  direction cosines to obtain a new vector normal to the  
9  
10 molecular plane. The projection of this vector onto the laboratory Z-axis then provides the  
11  
12 absolute orientational angle,[8, 48] which is determined to be  $\varphi = 74^\circ$ , as shown in Figure  
13  
14  
15 12b for isopropanol at STO (100) interfaces.  
16  
17



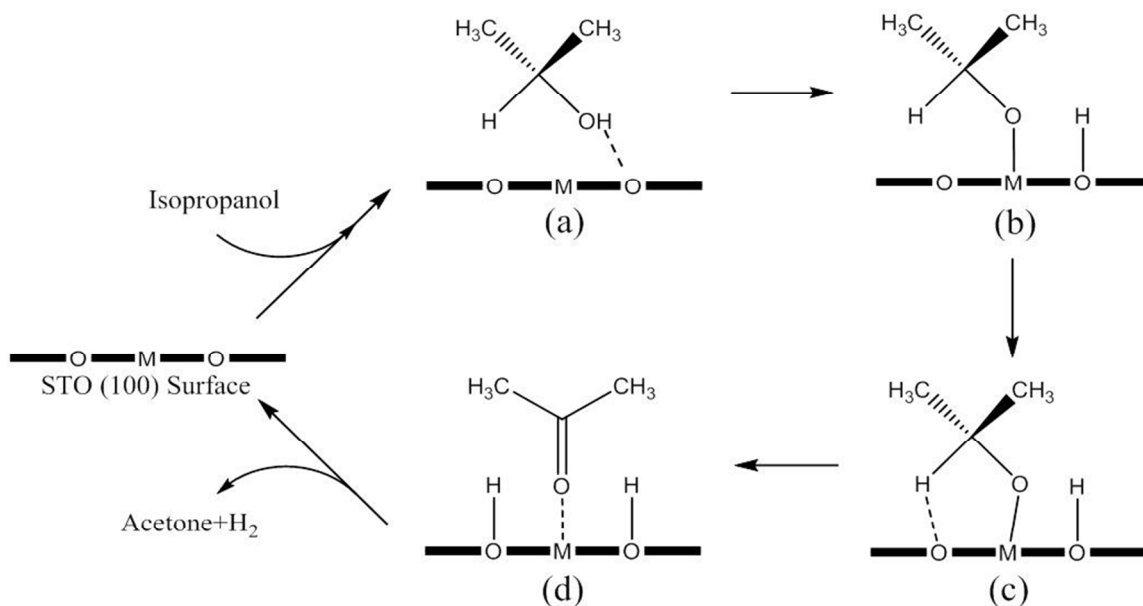
18  
19  
20  
21  
22  
23  
24  
25  
26  
27  
28  
29  
30  
31  
32  
33  
34  
35 Figure 12. Rotation of isopropanol to the laboratory frame. Angles between the surface normal  
36  
37 and various unit vectors are shown as described in the text.  
38  
39  
40  
41

### 42 **Insight into Catalytic Selectivity**

43  
44 Since there is a 1:1 correspondence with the exposed (100) facets on the nanoparticles  
45  
46 and the (100) flat surface, we can rationalize the *measured* selectivity from kinetic  
47  
48 measurements though a molecular level picture *measured* with SFG. Our kinetic results in  
49  
50 Figure 4 clearly show that STO nanocubes with exposed (100) facets convert isopropanol to  
51  
52 acetone as the dominant product at elevated temperatures. The question is then why does  
53  
54 STO (100) preferentially form this product? This is addressed by turning to SFG data and  
55  
56  
57  
58  
59  
60

1  
2  
3 the orientational information extracted from it. Hereby, we propose a reaction mechanism of  
4  
5 isopropanol over STO (100) surface as illustrated in Scheme 2. Mechanistically, we find that the  
6  
7 first step is that on adsorption, isopropanol exists in an equilibrium between a protonated and a  
8  
9 deprotonated species illustrated in step a) of Scheme 2. This is evidenced by INS data (Figure 8)  
10  
11 and the existence of two species in the SFG spectrum (Figure 10). The deprotonated species  
12  
13 assumes an orientation at the interface such that the methine (-CH) group is pointed towards the  
14  
15 STO surface as sketched in step Scheme 2b). Since we know from kinetic measurements that  
16  
17 acetone is produced as the dominant product and that abstraction of the hydrogen atom from the  
18  
19 central carbon in isopropanol has to occur to form acetone, it is reasonable to consider that at  
20  
21 elevated temperatures, the energetic barrier for abstraction of this proton is overcome at elevated  
22  
23 temperatures (step c) and thus producing acetone at the interface, which can subsequently desorb  
24  
25 (step d). This scheme is supported by INS measurements showing the existence of acetone at  
26  
27 STO (100) nanocube surfaces post reaction. This also agrees with our recent work on CeO<sub>2</sub> (100)  
28  
29 surfaces, where the dominant product is known to be propylene and the adsorbed isopropanol  
30  
31 molecules are assumed a different orientation, in which methyl groups are in closer proximity to  
32  
33 the surface.[8] For the case of CeO<sub>2</sub>, we showed previously that the molecule is arranged such  
34  
35 that a proton from a methyl group is pointed towards the CeO<sub>2</sub> (100). Notably, isopropanol  
36  
37 assumes a pre-reaction geometry where this critical proton is pointed towards the STO (100)  
38  
39 interface in an analogous way to the results previously reported by our group for CeO<sub>2</sub> (100).  
40  
41 Through the combination of these complimentary techniques, we have shown how simple  
42  
43 structural arguments can explain the selectivity in heterogeneous catalysis of well-defined  
44  
45 systems. Thus, these results show clearly that the selectivity of the catalyst is at least in part  
46  
47 dictated by the adsorption geometry of the molecule to the interface of interest. This is a  
48  
49  
50  
51  
52  
53  
54  
55  
56  
57  
58  
59  
60

chemically intuitive argument to describe the specificity of a given catalyst, but raises questions as to what drives the molecules to take on different orientations for different surfaces with the same surface indices. Continued work will aim to address this question to gain a predictive understanding of chemical catalysis.



Scheme 2. Proposed reaction mechanism of isopropanol conversion over SrTiO<sub>3</sub> (100) surface.

## Conclusions

The current work is the first report that combines the spectroscopic studies (INS, SFG) with kinetic investigations over Strontium Titanate perovskite catalysts. Here, we carried out a detailed study with isopropanol conversion as a model reaction. The steady state kinetic investigation illustrates the cubic STO, with (100) facet exposed, preferentially product acetone via dehydrogenation route. Meanwhile, the combination of inelastic neutron spectroscopy and sum frequency generation spectroscopy provided information regarding the surface adsorbate at a molecular level. To be specific, isopropanol adsorbed with a geometry of -CH group pointing towards the STO (100) surface thus assuming a pre-reaction geometry that ultimately drives the selectivity of the catalyst. Such orientation leads to higher acetone

1  
2  
3 production selectivity by deprotonation, which is consistent with kinetic observation. Comparing  
4  
5 these two surfaces, which have different reaction products, allows us to understand the role the  
6  
7 adsorbed molecules and their geometry on in driving catalytic selectivity. The implication is that  
8  
9 the catalytic performance is strongly surface-orientation dependent even at low temperature  
10  
11 conditions. Future work may focus on addressing the question as to what gives rise to the  
12  
13 differences in orientation to gain a predictive understanding of chemical catalysis.  
14  
15  
16  
17  
18  
19  
20  
21

## 22 ASSOCIATED CONTENT

23 Supporting information includes AFM topography, vibrational modes of isopropanol, and  
24  
25 reference SFG spectra. This material is available free of charge via the Internet at  
26  
27 <http://pubs.acs.org>.  
28  
29  
30  
31

## 32 AUTHOR INFORMATION

### 33 34 **Corresponding Authors**

35  
36  
37 \*Benjamin Doughty, Email: [doughtybl@ornl.gov](mailto:doughtybl@ornl.gov)

38  
39 \*Daniel A. Lutterman, Email: [luttermanda@ornl.gov](mailto:luttermanda@ornl.gov)

### 40 41 **Author Contributions**

42  
43  
44 The manuscript was written through contributions of all authors. All authors have given approval  
45  
46 to the final version of the manuscript.  
47  
48

### 49 50 **Acknowledgements**

51  
52 This work was supported by the U.S. Department of Energy, Office of Science, Basic Energy  
53  
54 Sciences, Chemical Sciences, Geosciences, and Biosciences Division (ST, MKK, BD, Y-ZM,  
55  
56 and DAL). DL and HNL were supported by U.S. Department of Energy, Office of Science,  
57  
58  
59  
60

1  
2  
3 Basic Energy Sciences, Materials Sciences and Engineering Division and prepared samples.  
4  
5  
6 Neutron vibrations spectroscopy (YC, LLD) research used resources at the Spallation Neutron  
7  
8 Source, a DOE Office of Science User Facility operated by the Oak Ridge National Laboratory.  
9  
10  
11 MG was funded by a summer Science Undergraduate Laboratory Internships (SULI) award at  
12  
13 Oak Ridge National Laboratory.  
14

### 15 Reference:

- 16
- 17
- 18 1. Corma, A.; Serra, J. M.; Serna, P.; Moliner, M., *J. Catal.* 2005, *232*, 335-341.
- 19 2. Hinde, C. S.; Ansovini, D.; Wells, P. P.; Collins, G.; Aswegen, S. V.; Holmes, J. D.; Hor, T.  
20 S. A.; Raja, R., *ACS Catal.* 2015, *5*, 3807-3816.
- 21 3. Lee, I.; Delbecq, F.; Morales, R.; Albiter, M. A.; Zaera, F., *Nat. Mater.* 2009, *8*, 132-138.
- 22 4. An, K.; Somorjai, G. A., *ChemCatChem* 2012, *4*, 1512-1524.
- 23 5. Li, J.; Kazakov, A.; Dryer, F. L., *J. Phys. Chem. A* 2004, *108*, 7671-7680.
- 24 6. Turek, W.; Krowiak, A., *Appl. Catal. A Gen.* 2012, *417-418*, 102-110.
- 25 7. Kamiguchi, S.; Okumura, K.; Nagashima, S.; Chihara, T., *Mater. Res. Bull.* 2015, *72*, 188-  
26 190.
- 27 8. Doughty, B.; Goverapet Srinivasan, S.; Bryantsev, V. S.; Lee, D.; Lee, H. N.; Ma, Y.-Z.;  
28 Lutterman, D. A., *J. Phys. Chem. C* 2017, *121*, 14137-14146.
- 29 9. Foo, G. S.; Polo-Garzon, F.; Fung, V.; Jiang, D.-e.; Overbury, S. H.; Wu, Z., *ACS Catal.*  
30 2017, *7*, 4423-4434.
- 31 10. Prince, E., *Appl. Spectrosc. Rev.* 2004, *34*, 159-172.
- 32 11. Stewart F. Parker, P. C., *Johnson Matthey Technol. Rev.* 2016, *60*, 132-144.
- 33 12. Wang, H.-F.; Gan, W.; Lu, R.; Rao, Y.; Wu, B.-H., *Int. Rev. Phys. Chem.* 2005, *24*, 191-256.
- 34 13. Kataoka, S.; Cremer, P. S., *J. Am. Chem. Soc.* 2006, *128*, 5516-5522.
- 35 14. Shen, Y. R., *J. Phys. Chem. C* 2012, *116*, 15505-15509.
- 36 15. Shen, Y. R., *Ann. Rev. Phys. Chem.* 2013, *64*, 129-150.
- 37 16. Jang, J. H.; Lydiatt, F.; Lindsay, R.; Baldelli, S., *J. Phys. Chem. A* 2013, *117*, 6288-6302.
- 38 17. Liu, A.-a.; Liu, S.; Zhang, R.; Ren, Z., *J. Phys. Chem. C* 2015, *119*, 23486-23494.
- 39 18. Liu, S.; Liu, A.-a.; Wen, B.; Zhang, R.; Zhou, C.; Liu, L.-M.; Ren, Z., *J. Phys. Chem. Lett.*  
40 2015, *6*, 3327-3334.
- 41 19. Wang, H.-F., *Prog. Surf. Sci.* 2016, *91*, 155-182.
- 42 20. Vanselous, H.; Stingel, A. M.; Petersen, P. B., *J. Phys. Chem. Lett.* 2017, *8*, 825-830.
- 43 21. Rabuffetti, F. A.; Kim, H.-S.; Enterkin, J. A.; Wang, Y.; Lanier, C. H.; Marks, L. D.;  
44 Poepelmeier, K. R.; Stair, P. C., *Chem. Mater.* 2008, *20*, 5628-5635.
- 45 22. Lee, H. N.; Christen, H. M.; Chisholm, M. F.; Rouleau, C. M.; Lowndes, D. H., *Nature*  
46 2005, *433*, 395-399.
- 47 23. Seeger, P. A.; Daemen, L. L.; Larese, J. Z., *Nucl. Instrum. Methods Phys. Res., Sect. A* 2009,  
48 *604*, 719-728.
- 49 24. Doughty, B.; Yin, P.; Ma, Y.-Z., *Langmuir* 2016, *32*, 8116-8122.
- 50 25. Voylov, D. N.; Holt, A. P.; Doughty, B.; Bocharova, V.; Meyer, H. M.; Cheng, S.; Martin,  
51 H.; Dadmun, M.; Kisliuk, A.; Sokolov, A. P., *ACS Macro Lett.* 2017, *6*, 68-72.  
52  
53  
54  
55  
56  
57  
58  
59  
60

- 1
  - 2
  - 3
  - 4
  - 5
  - 6
  - 7
  - 8
  - 9
  - 10
  - 11
  - 12
  - 13
  - 14
  - 15
  - 16
  - 17
  - 18
  - 19
  - 20
  - 21
  - 22
  - 23
  - 24
  - 25
  - 26
  - 27
  - 28
  - 29
  - 30
  - 31
  - 32
  - 33
  - 34
  - 35
  - 36
  - 37
  - 38
  - 39
  - 40
  - 41
  - 42
  - 43
  - 44
  - 45
  - 46
  - 47
  - 48
  - 49
  - 50
  - 51
  - 52
  - 53
  - 54
  - 55
  - 56
  - 57
  - 58
  - 59
  - 60
26. Weeraman, C.; Yatawara, A. K.; Bordenyuk, A. N.; Benderskii, A. V., *J. Am. Chem. Soc.* 2006, *128*, 14244-14245.
27. Chen, S.-L.; Fu, L.; Gan, W.; Wang, H.-F., *J. Chem. Phys.* 2016, *144*, 034704.
28. Enterkin, J. A.; Poeppelmeier, K. R.; Marks, L. D., *Nano Lett.* 2011, *11*, 993-997.
29. Thommes, M.; Kaneko, K.; Neimark Alexander, V.; Olivier James, P.; Rodriguez-Reinoso, F.; Rouquerol, J.; Sing Kenneth, S. W., Physisorption of gases, with special reference to the evaluation of surface area and pore size distribution (IUPAC Technical Report). In *Pure and Applied Chemistry*, 2015; Vol. 87, p 1051.
30. Kenneth S. W. Sing, R. T. W., *Adsorpt. Sci. Technol.* 2004, *22*, 773-782.
31. Ouqour, A.; Coudurier, G.; Vedrine, J. C., *J. Chem. Soc., Faraday Trans.* 1993, *89*, 3151-3155.
32. Taylor, E. A.; Griffin, G. L., *J Phys Chem-US* 1988, *92*, 477-481.
33. Park, Y. K.; Aghalayam, P.; Vlachos, D. G., *J. Phys. Chem. A.* 1999, *103*, 8101-8107.
34. Brandt, K.; Chiu, M. E.; Watson, D. J.; Tikhov, M. S.; Lambert, R. M., *J. Phys. Chem. C.* 2012, *116*, 4605-4611.
35. Badlani, M.; Wachs, I. E., *Catal. Lett.* 2001, *75*, 137-149.
36. Kulkarni, D.; Wachs, I. E., *Appl. Catal. A. Gen.* 2002, *237*, 121-137.
37. Finocchio, E.; J. Willey, R.; Busca, G.; Lorenzelli, V., *J. Chem. Soc., Faraday Trans.* 1997, *93*, 175-180.
38. Rekoske, J. E.; Barteau, M. A., *J. Catal.* 1997, *165*, 57-72.
39. Trikalitis, P. N.; Pomonis, P. J., *Appl. Catal. A. Gen.* 1995, *131*, 309-322.
40. de Beer, A. G. F.; Roke, S., *Phys. Rev. B.* 2009, *79*, 155420.
41. Yu, Y.; Wang, Y.; Hu, N.; Lin, K.; Zhou, X.; Liu, S., *J. Raman Spectrosc.* 2014, *45*, 259-265.
42. Lu, R.; Gan, W.; Wu, B.-h.; Zhang, Z.; Guo, Y.; Wang, H.-f., *J. Phys. Chem. B* 2005, *109*, 14118-14129.
43. Gobrogge, E. A.; Woods, B. L.; Walker, R. A., *Farad. Discuss.* 2013, *167*, 309-327.
44. Tian, C. S.; Shen, Y. R., *Surf. Sci. Rep.* 2014, *69*, 105-131.
45. Jang, J. H.; Lydiatt, F.; Lindsay, R.; Baldelli, S., *J. Phys. Chem. A.* 2013, *117*, 6288-6302.
46. Kett, P. J. N.; Casford, M. T. L.; Davies, P. B., *Mol. Phys.* 2013, *111*, 175-187.
47. Dodge, M. J., "Refractive Index" in *Handbook of Laser Science and Technology, Volume IV, Optical Materials: Part 2*. CRC Press: Boca Raton, 1986.
48. Rao, Y.; Comstock, M.; Eisenthal, K. B., *J. Phys. Chem. B* 2006, *110*, 1727-1732.

## TOC Graphic

